An 8-node assumed strain element with explicit integration for isotropic and laminated composite shells

K. D. Kim†

School of Civil Engineering, Asian Institute of Technology, P.O. Box 4 Klongluang, Pathumthani, 12120, Thailand

T. H. Park‡

Department of Civil and Environmental Engineering, Hanyang University, Seoul, Korea

Abstract. Formulation of an 8 nodes assumed strain shell element is presented for the analysis of shells. The stiffness matrix based on the Mindlin-Reissner theory is analytically integrated through the thickness. The element is free of membrane and shear locking behavior by using the assumed strain method such that the element performs very well in modeling of thin shell structures. The material is assumed to be isotropic and laminated composite. The element has six degrees of freedom per node and can model the stiffened plates and shells. A great number of numerical testing carried out for the validation of present 8 node shell element are in good agreement with references.

Key words: 8-node shell; assumed strain; laminated composite.

1. Introduction

Many shell element formulations have been based on so-called 'degenerate' models introduced by Ahamed *et al.* (1970) Whilst such elements are capable of dealing with thick plates and shell problems, their performance deteriorates rapidly as the thickness becomes smaller, which is due to the phenomenon called the locking. As commonly accepted, two kinds of locking phenomena may occur in curved shear flexible bending element, namely shear locking and membrane locking. While the shear locking may possibly occur in both flat and curved shear flexible bending element, the membrane locking occurs only in curved thin shell. The efforts by many investigators have been directed at overcoming the locking problem in Mindlin-Reissner type elements, thus rendering them effective and reliable for thin plate and shell applications as well. Bathe and Dvorkin (1986) proposed an eight-node shell element, named as MITC8, that avoids membrane and shear locking. The strain tensor was expressed in terms of the covariant components and covariant base vectors. The performance of this element was quite satisfactory and suggested the promising results in very complex shell structures. Huang and Hinton (1986) developed a 9 node assumed strain shell element

---

† Associate Professor
‡ Assistant Professor

(QUAD9**). They used an enhanced interpolation of the transverse shear strains in the natural coordinate system to overcome the shear locking problems. An enhanced interpolation of the membrane strains was used in the local Cartesian coordinate system to avoid membrane locking behavior. Lakshminaryana and Kailashi (1989) presented an eight node shell element (QUAD8**) which is free of locking. In order to resolve the locking problem, they used appropriately chosen interpolation functions based Hinton and Huang's concept. Choi and Yoo (1990) present a geometrically nonlinear 8 nodes shell element. They used an enhanced interpolation of transverse shear strain in the natural coordinates, reduced integration in membrane strains and selective addition of the nonconforming displacement modes. Kebari and Cassell (1992) have developed 9 node shell element based on a co-rotational method employing stabilization techniques. The shell element used the reduced integration to avoid locking and shows good performance with references. Ma and Kanok-Nukulchai (1989) developed a 9 node assumed strain shell element based on the desirable displacement concepts and Lee and Kanok-Nukulchai (1998) extended Ma's concept to the laminated composite shells. The solution showed good agreement with references. Kim *et al.* (1998) and Kim and Vojiadjis (1999) presented 8 node nonlinear composite shell element. In order to eliminate locking behavior in the above shell element, the energy control formulation is used based on the covariant base vectors which are determined at Gauss points. The shell element based on co-rotational method is taken into account finite rotations as well.

A great number of 9 node shell element formulation are presented up to date and showed good performance whereas only few 8 node shell element formulations are presented and performance are not good as 9 node shell elements. The objective of this paper is to present a new formulation of explicitly integrated 8 node shell element, which is further improved shell element presented by Kim *et al.* (1998). In order to eliminate both the shear locking and also membrane locking, the assumed strain method developed by Ma and Kanok-Nukulchai (1989) for the 9 node shell element is applied in the natural coordinate. The present shell element with full integration has the correct rank without zero energy modes and passes necessary testing for the reliability. The shell element can model both isotropic and anisotropic composite material. By using six degrees of freedom per node, the present element can model the stiffened plate and shell structures. The shell element showed very good performance compared with references using the different assumed strain methods in 8 nodes shell element by Bathe and Dvorkin (1986) and Lakshminaryana and Kailashi (1989). A few selected examples are presented for the validation of the present shell element from the various problems analyzed and compared with references.

2. Shell element formulation

2.1 Geometry of shell element

The eight node shell element shown in Fig. 1 is described by the relation between local (r, s, t) and natural curvilinear co-ordinate (ξ, η, ζ) established by base vectors. The midsurface is described by two non-dimensional coordinates ξ, η and the axis ζ is normal to the shell midsurface. The origin of the curvilinear coordinate system is set to the center of each element, however in general this coordinate system is not orthogonal. Hence the local orthogonal coordinate system (r, s, t) at the center of the element is constructed. The (r, s) and (ξ, η) surface are coplanar. The base vector (V_r, V_s, V_t) which are tangential to the local co-ordinates are defined as follows:

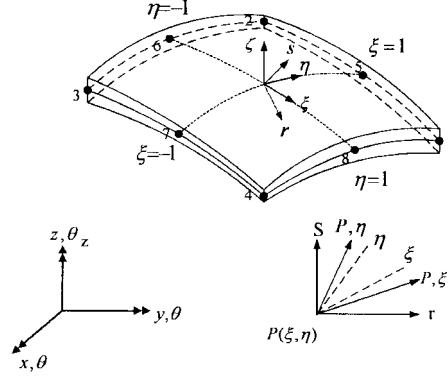Fig. 1 Mid-surface geometry and local coordinate of 8 node shell element

$$V_t = (\overline{V}_\xi \times \overline{V}_\eta)/|(\overline{V}_\xi \times \overline{V}_\eta)|$$

$$V_s = ((V_t \times \overline{V}_\xi) + \overline{V}_\eta)/|((V_t \times \overline{V}_\xi) + \overline{V}_\eta)|$$

$$V_r = V_s \times V_t \tag{1}$$

where $\overline{V}_\xi$ and $\overline{V}_\eta$ are the unit covariant base vectors tangential to ξ and η.

$$\overline{V}_\xi = \frac{\partial P}{\partial \xi} = \sum_{i=1}^{8} \frac{\partial H^i}{\partial \xi} P^i / \left| \frac{\partial H^i}{\partial \xi} P^i \right|$$

$$\overline{V}_\eta = \frac{\partial P}{\partial \eta} = \sum_{i=1}^{8} \frac{\partial H^i}{\partial \eta} P^i / \left| \frac{\partial H^i}{\partial \eta} P^i \right|$$

$$\tag{2}$$

The position vector of point $P(r, s, t)$ located at distance t from the midsurfaceis given by

$$P = \sum_{i=1}^{8} H^i(\xi, \eta) \overline{P}^i + t V_t \tag{3}$$

i.e.,

$$\begin{Bmatrix} x \\ y \\ z \end{Bmatrix}_P = \sum_{i=1}^{8} H^i \begin{Bmatrix} \overline{x}_i \\ \overline{y}_i \\ \overline{z}_i \end{Bmatrix} + t \begin{Bmatrix} V_t(1) \\ V_t(2) \\ V_t(3) \end{Bmatrix}_P \tag{4}$$

where $H^i (i = 1, \cdots, 8)$ is the shape function and $\overline{P}^i$ is the position vector of node i on the mid-surface. The linear coordinate t lies in the range $-h/2 \le t \le h/2$, and the thickness h is directly interpolated from the nodes.

$$h = \sum_{i=1}^{8} H^i h^i \tag{5}$$

It is important to note that V_t is normal to the midsurface of the element and it is independent of top and bottom nodal coordinates. The approximation introduced by ignoring the variation of Jacobian through the thickness would not violate rigid body rotation requirement if V_t is used instead of V_t^i in the definition of the geometry of the elements.

2.2 Displacement fields

The six degrees of freedom per node are interpolated over the midsurface in accordance with

$$\begin{Bmatrix} \overline{U} \\ \overline{V} \\ \overline{W} \end{Bmatrix} = \sum_{i=1}^{8} H^i(\xi, \eta) \begin{Bmatrix} \overline{U}^i \\ \overline{V}^i \\ \overline{W}^i \end{Bmatrix} \qquad \begin{Bmatrix} \theta_x \\ \theta_y \\ \theta_z \end{Bmatrix} = \sum_{i=1}^{8} H^i(\xi, \eta) \begin{Bmatrix} \theta_x^i \\ \theta_y^i \\ \theta_z^i \end{Bmatrix} \tag{6}$$

The traditional formulation of shells consists of converting global displacement values to the local coordinate system and then interpolated at the Gauss points. Present formulation, initiated by Kebari and Cassel (1992) first interpolates global displacement values at Gauss points and then transfer them to local coordinate. This method reduces the computational time.

The local motion of any point $p(r, s, t)$ is approximately defined by the Mindlin-Reissner theory based on the first order approximation.

$$u = \overline{u} + t\varphi_s$$
$$v = \overline{v} - t\varphi_r$$
$$w = \overline{w}(r, s) \tag{7}$$

The local variables can be interpolated as the global six degrees of freedom per node over the mid-surface in accordance with

$$\begin{Bmatrix} \overline{u} \\ \overline{v} \\ \overline{w} \end{Bmatrix} = [T]^T \begin{Bmatrix} \overline{U} \\ \overline{V} \\ \overline{W} \end{Bmatrix} \qquad \begin{Bmatrix} \varphi_s \\ \varphi_r \\ 0 \end{Bmatrix} = \begin{bmatrix} 0 & 1 & 0 \\ -1 & 0 & 0 \\ 0 & 0 & 0 \end{bmatrix} [T]^T \begin{Bmatrix} \theta_x \\ \theta_y \\ \theta_z \end{Bmatrix} \tag{8}$$

where the direction cosine of the new local axes (r, s, t) with respect to the global axes (x, y, z) are defined by $[T]$ matrix.

$$[T]^T = \begin{bmatrix} l_r & m_r & n_r \\ l_s & m_s & n_s \\ l_t & m_t & n_t \end{bmatrix} = \begin{Bmatrix} V_r^T \\ V_s^T \\ V_t^T \end{Bmatrix} \tag{9}$$

Combining equations from (6) to (9), the global translation by the transformation from local to global can be written using the definition of position vector.

$$U = \sum_{i=1}^{8} H^i(\xi, \eta) \overline{U}^i + t\Theta\theta \tag{10}$$

where $\overline{U}^i(\overline{U}^i, \overline{V}^i, \overline{W}^i)$ and $\boldsymbol{\theta}(\theta_x, \theta_y, \theta_z)$ are the global displacement and rotation vector theta which is a function of nodal values as defined in Eq. (6) on the mid-surface respectively. The transformation matrix $\boldsymbol{\Theta}$ has the form.

$$
\boldsymbol{\Theta} \;=\; \begin{bmatrix} 0 & n_t & -m_t \\ -n_t & 0 & l_t \\ m_t & -l_t & 0 \end{bmatrix}
\tag{11}
$$

where l_t, m_t, n_t are components of the unit vector $\boldsymbol{V}_t$.

2.3 Strain-displacement relationship

In order to express the strains in terms of nodal displacements, the local strain components should be transformed into the global co-ordinates. By using the interpolation functions, the strain and displacement relationships are obtained as follows:

The linear strain-displacement relations in local Cartesian orthogonal coordinate systems are given by the usual equations.

$$
e_{rr} \;=\; \frac{\partial \overline{u}}{\partial r} + t\frac{\partial \varphi_s}{\partial r}
$$

$$
e_{ss} \;=\; \frac{\partial \overline{v}}{\partial s} - t\frac{\partial \varphi_r}{\partial s}
$$

$$
e_{rs} \;=\; \frac{\partial \overline{v}}{\partial r} + \frac{\partial \overline{u}}{\partial s} + t\left(\frac{\partial \varphi_s}{\partial r} - \frac{\partial \varphi_r}{\partial s}\right)
$$

$$
e_{rt} \;=\; \frac{\partial \overline{w}}{\partial r} + \varphi_s
$$

$$
e_{st} \;=\; \frac{\partial \overline{w}}{\partial s} - \varphi_r
\tag{12}
$$

The local displacement can be expressed in terms of local direction cosine, form Eq. (9) as

$$
\overline{u} \;=\; \boldsymbol{V}_r^T \overline{\boldsymbol{U}} \qquad \varphi_s = \boldsymbol{V}_s^T \boldsymbol{\theta}
\tag{13}
$$

where $\overline{\boldsymbol{U}} \;=\; \{\overline{U}, \overline{V}, \overline{W}\}$ and $\boldsymbol{\theta} \;=\; \{\theta_x, \theta_y, \theta_z\}$.

The local strain component is transformed in terms of global transitions.

$$
e_{rr} \;=\; \frac{\partial \overline{u}}{\partial r} + t\frac{\partial \varphi_s}{\partial r} \;=\; \boldsymbol{V}_r^T \frac{\partial \overline{\boldsymbol{U}}}{\partial r} + t\boldsymbol{V}_s^T \frac{\partial \boldsymbol{\theta}}{\partial r}
\tag{14}
$$

To compute the derivative of global displacements with respect to curvilinear system, the surface Jacobian [$\boldsymbol{J}$] separated from thickness variation is used because the surface Jacobian is approximately equal at all layers given by.

$$\left\{ \begin{array}{c} \dfrac{\partial}{\partial \xi} \\[3mm] \dfrac{\partial}{\partial \eta} \end{array} \right\} = \left[\begin{array}{cc} \dfrac{\partial r}{\partial \xi} & \dfrac{\partial s}{\partial \xi} \\[3mm] \dfrac{\partial r}{\partial \eta} & \dfrac{\partial s}{\partial \eta} \end{array} \right] \left\{ \begin{array}{c} \dfrac{\partial}{\partial r} \\[3mm] \dfrac{\partial}{\partial s} \end{array} \right\} = \left[\begin{array}{cc} \overline{V}_\xi V_r & \overline{V}_\xi V_s \\[2mm] \overline{V}_\eta V_r & \overline{V}_\eta V_s \end{array} \right] \left\{ \begin{array}{c} \dfrac{\partial}{\partial r} \\[3mm] \dfrac{\partial}{\partial s} \end{array} \right\} = [J] \left\{ \begin{array}{c} \dfrac{\partial}{\partial r} \\[3mm] \dfrac{\partial}{\partial s} \end{array} \right\} \tag{15}$$

Hence, using the inverse of the surface Jacobian matrix, the following relation is obtained.

$$\left\{ \begin{array}{c} \dfrac{\partial}{\partial r} \\[3mm] \dfrac{\partial}{\partial s} \end{array} \right\} = \dfrac{1}{[J]} \left[\begin{array}{cc} \overline{V}_\eta \overline{V}_s & -\overline{V}_\xi \overline{V}_s \\[2mm] -\overline{V}_\eta \overline{V}_r & \overline{V}_\xi \overline{V}_r \end{array} \right] \left\{ \begin{array}{c} \dfrac{\partial}{\partial \xi} \\[3mm] \dfrac{\partial}{\partial \eta} \end{array} \right\} = \left[\begin{array}{cc} \Gamma_{11} & \Gamma_{12} \\[2mm] \Gamma_{21} & \Gamma_{22} \end{array} \right] \left\{ \begin{array}{c} \dfrac{\partial}{\partial \xi} \\[3mm] \dfrac{\partial}{\partial \eta} \end{array} \right\} \tag{16}$$

where

$$\Gamma_{11} = \dfrac{\overline{V}_\eta V_s}{[J]} \quad \Gamma_{21} = \dfrac{-\overline{V}_\eta V_r}{[J]} \quad \Gamma_{12} = \dfrac{-\overline{V}_\xi V_s}{[J]} \quad \Gamma_{22} = \dfrac{\overline{V}_\xi V_r}{[J]} \tag{17}$$

After the transformation of Eq. (14) and the introduction of the interpolation functions, the strain can be calculated as,

$$e_{rr} = \Gamma_{11} V_r^T \dfrac{\partial \overline{U}}{\partial \xi} + \Gamma_{12} V_r^T \dfrac{\partial \overline{U}}{\partial \eta} + t\left(\Gamma_{11} V_s^T \dfrac{\partial \boldsymbol{\theta}}{\partial \xi} + \Gamma_{12} V_s^T \dfrac{\partial \boldsymbol{\theta}}{\partial \eta} \right)$$

$$= \Gamma_{11} V_r^T \sum_{i=1}^{8} \dfrac{\partial H^i}{\partial \xi} \overline{U}^i + \Gamma_{12} V_r^T \sum_{i=1}^{8} \dfrac{\partial H^i}{\partial \eta} \overline{U}^i + t\left(\Gamma_{11} V_s^T \sum_{i=1}^{8} \dfrac{\partial H^i}{\partial \xi} \boldsymbol{\theta}^i + \Gamma_{12} V_s^T \sum_{i=1}^{8} \dfrac{\partial H^i}{\partial \eta} \boldsymbol{\theta}^i \right) \tag{18}$$

Similarly, each strain terms based on the theory of first order shear deformation, the following strain-displacement relationship is obtained,

$$\left\{ \begin{array}{c} e_{rr} \\ e_{ss} \\ e_{rs} \end{array} \right\} = \sum_{i=1}^{8} \left[\left[\begin{array}{c} f^i V_r^T \\ g^i V_s^T \\ f^i V_s^T + g^i V_r^T \end{array} \right] + t \left[\begin{array}{c} f^i V_s^T \\ g^i V_r^T \\ g^i V_s^T - f^i V_r^T \end{array} \right] \right] \left\{ \begin{array}{c} \overline{U}^i \\ \boldsymbol{\theta}^i \end{array} \right\} = \sum_{i=1}^{8} \left[\boldsymbol{B}_m^i \quad t\boldsymbol{B}_b^i \right] \left\{ \begin{array}{c} \overline{U}^i \\ \boldsymbol{\theta}^i \end{array} \right\}$$

$$\left\{ \begin{array}{c} e_{rt} \\ e_{st} \end{array} \right\} = \sum_{i=1}^{8} \left[\begin{array}{cc} f^i V_t^T & H^i V_r^T \\ g^i V_t^T & -H^i V_s^T \end{array} \right] \left\{ \begin{array}{c} \overline{U}^i \\ \boldsymbol{\theta}^i \end{array} \right\} = \sum_{i=1}^{8} \left[\boldsymbol{B}_q^i \quad \boldsymbol{H}_q^i \right] \left\{ \begin{array}{c} \overline{U}^i \\ \boldsymbol{\theta}^i \end{array} \right\} \tag{19}$$

where

$$f^i = \Gamma_{11} \dfrac{\partial H^i}{\partial \xi} + \Gamma_{12} \dfrac{\partial H^i}{\partial \eta}$$

$$g^i = \Gamma_{21} \dfrac{\partial H^i}{\partial \xi} + \Gamma_{22} \dfrac{\partial H^i}{\partial \eta} \tag{20}$$

The above Eq. (19) can be rearranged as given in the following compact form, separating the membrane, bending and transverse shear strain terms respectively,

$$e_m = \sum_{i=1}^{8} B_m^i \overline{U}^i$$

$$e_b = \sum_{i=1}^{8} B_b^i \theta^i$$

$$e_q = \sum_{i=1}^{8} \left[B_q^i \ H_q^i \right] \begin{Bmatrix} \overline{U}^i \\ \theta^i \end{Bmatrix} \tag{21}$$

where B_m^i, B_b^i and $[B_q^i \ H_q^i]$ are the strain-displacement matrix due to membrane, bending and transverse shear, respectively.

2.4 Transverse shear locking

Various methods have been proposed by a number of researchers to overcome the shear locking of thin plates and shells as presented in introduction. Among various method presented, the assumed strain method has been successfully used for the finite element formulations based on Mindlin-Reissner theory in order to overcome shear locking problem. To overcome the shear locking problems in thin shell many researchers used both reduced integration and selective integration. However such methods have rank deficiency and zero energy modes. In order to solve this problem, the assumed strain method using the full integration is adopted in the present study to eliminate not only locking problems but also zero energy modes. Bathe and Dvorkin (1986) interpolated the transverse shear strains in terms of covariant components to remove the shear locking in 8-node shell element by using 5 sampling points. Lakshminaryana and Kailashi (1989) interpolated the transverse shear strains in the natural coordinates and also used 5 sampling points. However, in the current element, the transverse shear strain fields are interpolated using 6 sampling points in the natural coordinates.

The transverse shear strain components are converted to the natural coordinate system by the following relation.

$$\varepsilon_{\alpha\beta} = \frac{\partial x^i}{\partial \alpha} \frac{\partial x^i}{\partial \beta} \varepsilon_{ij} \tag{22}$$

where $\varepsilon_{\alpha\beta}$ is the strain tensor in the natural coordinate system and ε_{ij} is the strain tensor in the local coordinate system. Then transverse shear strains in the two coordinate systems can be expressed as follows (see appendix 1):

$$\begin{Bmatrix} \gamma_{\xi\varsigma} \\ \gamma_{\eta\varsigma} \end{Bmatrix} = \frac{h}{2} \begin{bmatrix} \dfrac{\partial r}{\partial \xi} & \dfrac{\partial s}{\partial \xi} \\ \dfrac{\partial r}{\partial \eta} & \dfrac{\partial s}{\partial \eta} \end{bmatrix} \begin{Bmatrix} \varepsilon_{rt} \\ \varepsilon_{st} \end{Bmatrix} = \begin{bmatrix} J_{11} & J_{12} \\ J_{21} & J_{22} \end{bmatrix} \begin{Bmatrix} \varepsilon_{rt} \\ \varepsilon_{st} \end{Bmatrix} \tag{23}$$

The transverse shear strains ($\gamma_{\xi\varsigma}, \gamma_{\eta\varsigma}$) in the natural coordinates are calculated at the six sampling points and interpolated by the functions given in Eq. (24). The desired transverse shear strain is obtained by transforming back to local coordinate using Eq. (25).
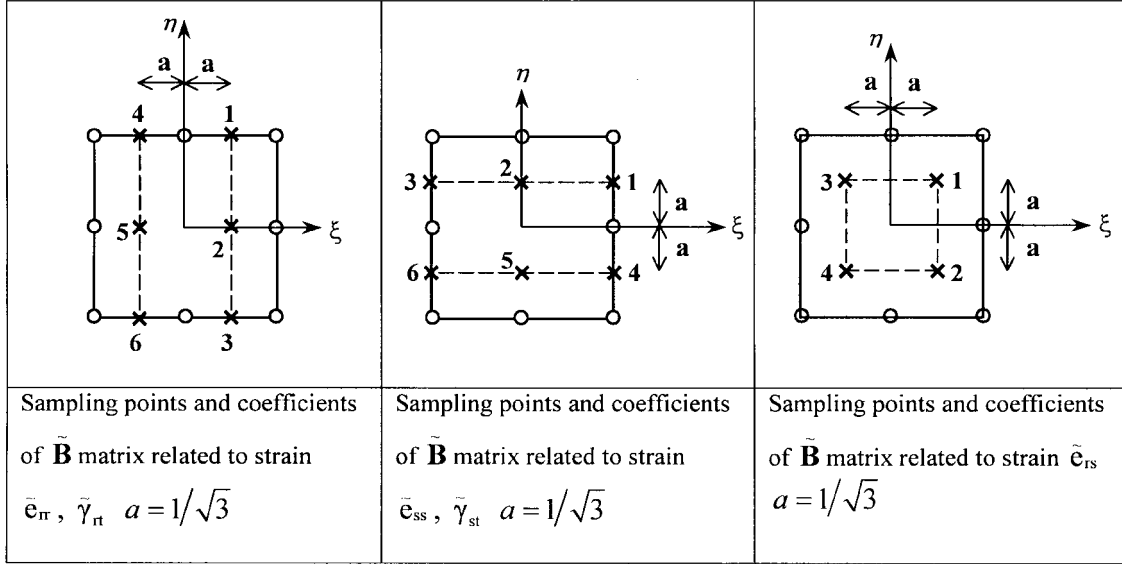
Sampling points and coefficients of $\tilde{\mathbf{B}}$ matrix related to strain $\bar{e}_{rr}$, $\bar{\gamma}_{rt}$ $a = 1/\sqrt{3}$	Sampling points and coefficients of $\tilde{\mathbf{B}}$ matrix related to strain $\bar{e}_{ss}$, $\bar{\gamma}_{st}$ $a = 1/\sqrt{3}$	Sampling points and coefficients of $\tilde{\mathbf{B}}$ matrix related to strain $\tilde{e}_{rs}$ $a = 1/\sqrt{3}$

Fig. 2 Sampling points

$$\tilde{\gamma}_{\xi\varsigma} = \sum_{i=1}^{2}\sum_{j=1}^{3} P_i(\xi)Q_j(\eta)\gamma_{\xi\varsigma}^{ij} \qquad \tilde{\gamma}_{\eta\varsigma} = \sum_{i=1}^{2}\sum_{j=1}^{3} P_i(\eta)Q_j(\xi)\gamma_{\eta\varsigma}^{ij} \tag{24}$$

$$\left\{\begin{matrix} \tilde{\varepsilon}_{rt} \\ \tilde{\varepsilon}_{st} \end{matrix}\right\} = \begin{bmatrix} \dfrac{\partial\xi}{\partial r} & \dfrac{\partial\eta}{\partial r} \\ \dfrac{\partial\xi}{\partial s} & \dfrac{\partial\eta}{\partial s} \end{bmatrix} \left\{\begin{matrix} \tilde{\gamma}_{\xi\varsigma} \\ \tilde{\gamma}_{\eta\varsigma} \end{matrix}\right\} = \begin{bmatrix} \Gamma_{11} & \Gamma_{12} \\ \Gamma_{21} & \Gamma_{22} \end{bmatrix} \left\{\begin{matrix} \tilde{\gamma}_{\xi\varsigma} \\ \tilde{\gamma}_{\eta\varsigma} \end{matrix}\right\} = \begin{bmatrix} \tilde{\mathbf{B}}_q^i & \tilde{\mathbf{H}}_q^i \end{bmatrix} \left\{\begin{matrix} \overline{U}^i \\ \boldsymbol{\theta}^i \end{matrix}\right\} \tag{25}$$

where i and j in Eq. (24) indicate the sampling points.

On the other hand, in order to control the transverse shear energy for thin plate and shell using reduced integration, the shear locking factor denoted by Ψ has been defined using the energy balance formulation as

$$\Psi = \frac{\phi h^2}{1 - v}\left(\frac{1}{e_a^2} + \frac{1}{e_b^2}\right) \tag{26}$$

where e_a and e_b are edge length and width of the element and ϕ is a stiffness control constant which is determined numerically Kim and Vojiadjis (1999). For an element of arbitrary shape, e_a^2 and e_b^2 can be replaced by,

$$\begin{aligned} e_a^2 &= \mathbf{V}_r \cdot \mathbf{V}_r \\ e_b^2 &= \mathbf{V}_s \cdot \mathbf{V}_s \end{aligned} \tag{27}$$

where the covariant base vectors ($\mathbf{V}_r$, $\mathbf{V}_s$) given in Eq. (1) are determined at the Gauss points. For thick plate and shell elements with a shear locking factor greater than unity, this factor is reset as

one, since such elements do not require the use of any shear locking factors.

2.5 Membrane locking

The problem of membrane locking has been reported in many literatures (Belytschko *et al.* 1989 and Huang and Hinton, 1986), in addition to the shear locking in modeling of the curved shell problems. The membrane locking in curved shell elements occur due to the instability of simulating adequate membrane strains. When serendipity element is used to model curved shells, the elements exhibit a tendency to produce spurious membrane effects under pure bending. This phenomenon is known as membrane locking and the effects can be improved by reduced integration. However, the reduced integration of an 8 node shell element does not give an accurate solution in highly curved shells in which the membrane effects are dominant. Lakshminaryana and Kailashi (1989) assumed the membrane strains in the local coordinates to remove the membrane locking and used 6 sampling points for $e_{\xi\eta}$. Bathe and Dvorkin (1986) assumed the inlayer strains in terms of covariant base vectors with 8 sampling points for the membrane strains. In the current element, the membrane strain fields are interpolated in the natural coordinates and compared with the results of the eight-node shell element by Bathe and Dvorkin, and Lakshminaryana and Kailashi in the numerical examples.

The membrane strains in the local coordinate are first converted to the natural coordinate based on Eq. (22). (see Appendix 2)

$$
\begin{Bmatrix} e_{\zeta\zeta} \\ e_{\eta\eta} \\ e_{\xi\eta} \end{Bmatrix} = \begin{bmatrix} \dfrac{\partial r}{\partial \xi}\dfrac{\partial r}{\partial \xi} & \dfrac{\partial s}{\partial \xi}\dfrac{\partial s}{\partial \xi} & 2\dfrac{\partial r}{\partial \xi}\dfrac{\partial s}{\partial \xi} \\ \dfrac{\partial r}{\partial \eta}\dfrac{\partial r}{\partial \eta} & \dfrac{\partial s}{\partial \eta}\dfrac{\partial s}{\partial \eta} & 2\dfrac{\partial s}{\partial \eta}\dfrac{\partial r}{\partial \eta} \\ \dfrac{\partial r}{\partial \xi}\dfrac{\partial r}{\partial \eta} & \dfrac{\partial s}{\partial \xi}\dfrac{\partial s}{\partial \eta} & \left(\dfrac{\partial r}{\partial \xi}\dfrac{\partial s}{\partial \eta} + \dfrac{\partial s}{\partial \xi}\dfrac{\partial r}{\partial \eta}\right) \end{bmatrix} \begin{Bmatrix} e_{rr} \\ e_{ss} \\ e_{rs} \end{Bmatrix} = \begin{bmatrix} J_{11}^2 & J_{12}^2 & 2J_{11}J_{12} \\ J_{21}^2 & J_{22}^2 & 2J_{21}J_{22} \\ J_{11}J_{21} & J_{12}J_{22} & J_{11}J_{22}+J_{21}J_{12} \end{bmatrix} \begin{Bmatrix} e_{rr} \\ e_{ss} \\ e_{rs} \end{Bmatrix} \quad (28)
$$

The assumed membrane strains in the natural coordinates ($\tilde{e}_{\xi\xi}, \tilde{e}_{\eta\eta}$) are calculated at six sampling points, and $\tilde{e}_{\xi\eta}$ is calculated at four sampling points shown in Fig. 2. The assumed natural strains $\tilde{e}_{\xi\xi}, \tilde{e}_{\eta\eta}$ have the same interpolation scheme as $\tilde{\gamma}_{\xi\varsigma}$ and $\tilde{\gamma}_{\eta\varsigma}$ respectively shown in Eq. (24). The interpolation of $\tilde{e}_{\xi\eta}$ is different due to having 4 points instead of 6 points and is given by,

$$
\tilde{e}_{\xi\eta} = \sum_{i=1}^{2}\sum_{j=1}^{2} P_i(\xi)P_j(\eta)\gamma_{\xi\eta}^{ij} \quad (29)
$$

The desired membrane strain is transformed from natural coordinate to local coordinate by inverse transformation of the Eq. (28) and expressed as the following relations.

$$
\begin{Bmatrix} \tilde{e}_{rr} \\ \tilde{e}_{ss} \\ \tilde{e}_{rs} \end{Bmatrix} = \begin{bmatrix} J_{11}^2 & J_{12}^2 & 2J_{11}J_{12} \\ J_{21}^2 & J_{22}^2 & 2J_{21}J_{22} \\ J_{11}J_{21} & J_{12}J_{22} & J_{11}J_{22}+J_{21}J_{12} \end{bmatrix}^{-1} \begin{Bmatrix} \tilde{e}_{\xi\xi} \\ \tilde{e}_{\eta\eta} \\ \tilde{e}_{\xi\eta} \end{Bmatrix} \quad (30)
$$

Table 1 Interpolation function for assumed natural strain fields

$\tilde{H}^i$	*Two point interpolation functions-P_i, P_j	*Three point interpolation functions-Q_j
1) $\sum\limits_{i=1}^{2}\sum\limits_{j=1}^{3} P_i(\xi)Q_j(\eta)$	$P_1(\xi) = \frac{1}{2}(1 + \sqrt{3}\xi)$	$Q_1(\eta) = \frac{1}{2}\eta(\eta + 1)$
2) $\sum\limits_{i=1}^{2}\sum\limits_{j=1}^{3} P_i(\eta)Q_j(\xi)$	$P_2(\xi) = \frac{1}{2}(1 + \sqrt{3}\xi)$	$Q_2(\eta) = 1 - \eta^2$
3) $\sum\limits_{i=1}^{2}\sum\limits_{j=1}^{2} P_i(\xi)P_j(\eta)$		$Q_3(\eta) = \frac{1}{2}\eta(\eta - 1)$

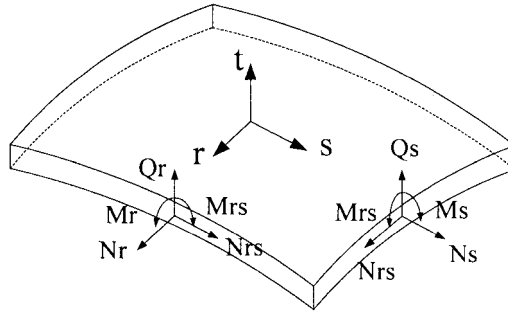*Note: $P(\eta)$ and $Q(\xi)$ can be obtain by a changing variables.

Fig. 3 Stress resultants of shell element

The assumed natural membrane strain can be expressed as follows:

$$\tilde{\boldsymbol{e}}_m = \sum_{i=1}^{8} \tilde{\boldsymbol{B}}_m^i \overline{\boldsymbol{U}}^i \tag{31}$$

2.6 Constitutive relation

The resultant membrane forces, moments and transverse shear forces are obtained by integration of stresses through the thickness. The directions of the strain resultants are shown in Fig. 3.

When the entire section is elastic, then the isotropic rigidity matrix reduces to the following form.

$$\begin{Bmatrix} \boldsymbol{N} \\ \boldsymbol{M} \\ \boldsymbol{Q} \end{Bmatrix} = \begin{bmatrix} h\boldsymbol{C}_e & 0 & 0 \\ 0 & \dfrac{h^3}{12}\boldsymbol{C}_e & 0 \\ 0 & 0 & \overline{\boldsymbol{A}} \end{bmatrix} \begin{Bmatrix} \boldsymbol{e}_m \\ \boldsymbol{e}_b \\ \boldsymbol{e}_q \end{Bmatrix} \tag{32}$$

where $\boldsymbol{N} = \{N_r, N_s, N_{rs}\}, \boldsymbol{M} = \{M_r, M_s, M_{rs}\}, \boldsymbol{Q} = \{Q_r, Q_s\}$.
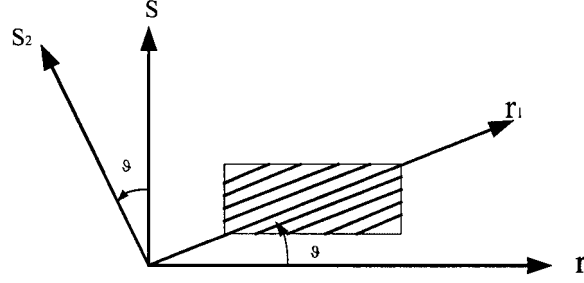
Fig. 4 Lamina coordinate

$$C_e = \frac{E}{1-v^2}\begin{bmatrix} 1 & v & 0 \\ 0 & 1 & 0 \\ 0 & 0 & (1-v)/2 \end{bmatrix} \qquad \overline{A} = \frac{5}{6}\begin{bmatrix} G & 0 \\ 0 & G \end{bmatrix} \tag{33}$$

The orthotropic stress strain relationship of anisotropic laminated composite for the k-th layer (Laminae Coordinate shown in Fig. 4) is given by appendix 3.

The resultant membrane forces (N), moments (M) and transverse shear forces (Q) acting on a laminated composite are obtained by integrating the stresses through the laminate thickness. The compact incremental constitutive relationship of the laminated composite are given as follows:

$$\begin{Bmatrix} N \\ M \\ Q \end{Bmatrix} = \begin{bmatrix} A & B & 0 \\ B & D & 0 \\ 0 & 0 & \overline{A} \end{bmatrix} \begin{Bmatrix} e_m \\ e_b \\ e_q \end{Bmatrix} \tag{34}$$

where

$$A = \sum_{k=1}^{NL} \overline{C}_{ij}^k (t_{k-1} - t_k)$$

$$B = \frac{1}{2}\sum_{k=1}^{NL} \overline{C}_{ij}^k (t_{k-1}^2 - t_k^2)$$

$$D = \frac{1}{3}\sum_{k=1}^{NL} \overline{C}_{ij}^k (t_{k-1}^3 - t_k^3)$$

$$\overline{A} = \frac{5}{6}\sum_{k=1}^{NL} \overline{C}_{ij}^k (t_{k-1} - t_k) \text{ for } i, j = 4, 5 \tag{35}$$

where NL is the total number of layers and the derivation of $\overline{C}_{ij}^k$ is shown in Appendix 3. In the case of laminated composite materials, there is a need to define adequately the effective transverse shear stiffness for a wide range of material properties and laminate geometry. Several methods have been suggested and stated that the displacement mode must also be considered in order to determine

effective shear modulus for laminated composite structures. Reddy (1987) developed the so-called layerwise theories, which use piecewise polynomial distribution (zig-zag function) of the membrane displacements in the thickness direction and provide a very good approximation of the transverse shear stresses. Rolfes and Rohwer (1997) developed a method based on the first-order shear deformation theory for calculating improved transverse shear stresses in laminated composite plates. The basic idea is to calculate the transverse shear stresses directly from the transverse shear forces by neglecting the influence of the membrane forces and assuming two cylindrical bending modes.

This is an area where further work is clearly needed, especially if the numerical models are used in the analysis of thick structures. The current study is mainly dealing with the linear response analysis. The Reissner's value of 5/6 is used for the transverse shear correction factor in the finite element formulations.

2.7 Element stiffness matrices

In practice Hook's law is only applicable to linear strain and hence the coefficients of constitutive tensor are constant. The following strain energy ($\widehat{U}_{st}$) is obtained using the linear strain assumption,

$$\widehat{U}_{st} = \frac{1}{2}\int \boldsymbol{\varepsilon}^T \widehat{\boldsymbol{D}} \boldsymbol{\varepsilon} \, \mathrm{d}V = \frac{1}{2} U^T [\tilde{\boldsymbol{B}}^T \widehat{\boldsymbol{D}} \tilde{\boldsymbol{B}} \mathrm{d}V] U = \frac{1}{2} U^T \boldsymbol{K}_e U \tag{36}$$

where $\widehat{\boldsymbol{D}}$ is elastic constant, $\tilde{\boldsymbol{B}}$ is strain displacement matrix and $U = \{\overline{U}, \boldsymbol{\theta}\}$.

The element stiffness matrix is written as follows:

$$\boldsymbol{K}_e^{ij} = \int_v (\boldsymbol{B}^i)^T \widehat{\boldsymbol{D}} \boldsymbol{B}^j dV$$

$$= \int_s \sum_{K=1}^{NL} \int_{t_{k-1}}^{t_k} \begin{bmatrix} \boldsymbol{B}_m^i & t\boldsymbol{B}_b^i \\ t\boldsymbol{B}_q^i & \boldsymbol{H}_q^i \end{bmatrix}^T \begin{bmatrix} \boldsymbol{C}_f & \boldsymbol{0} \\ \boldsymbol{0} & \boldsymbol{C}_s \end{bmatrix} \begin{bmatrix} \boldsymbol{B}_m^j & t\boldsymbol{B}_b^j \\ t\boldsymbol{B}_q^j & \boldsymbol{H}_q^j \end{bmatrix} dt dS \tag{37}$$

where $\boldsymbol{C}_f$ and $\boldsymbol{C}_s$ are elastic bending and transverse shear stiffness.

The element stiffness matrix is analytically integrated through the thickness. The stiffness of laminated composite is integrated over each layer. Finally the element stiffness matrix has on the reference-surface of shell (S).

$$K_e^{ij} = \int_s \begin{bmatrix} (\boldsymbol{B}_m^i)^T A \boldsymbol{B}_m^j + (\boldsymbol{B}_q^i)^T \overline{A} \boldsymbol{B}_q^j, & (\boldsymbol{B}_m^i)^T B \boldsymbol{B}_b^j + (\boldsymbol{B}_q^i)^T \overline{A} \boldsymbol{H}_q^j \\ (\boldsymbol{B}_b^i)^T B \boldsymbol{B}_m^j + (\boldsymbol{H}_q^i)^T \overline{A} \boldsymbol{B}_q^j, & (\boldsymbol{B}_b^i)^T D \boldsymbol{B}_b^j + (\boldsymbol{H}_q^i)^T \overline{A} \boldsymbol{H}_q^j \end{bmatrix} dS \tag{38}$$

To model stiffened plates and shells, the need for six degrees of freedom arises because the process of stiffness accumulation at any node lying on the junction must be carried out in a single reference frame. However, it is well-known that this creates problems associated with rotation about the normal to the shell mid-surface. Initially, this torsional degree of freedom was specified in global co-ordinates but this leads to singularity problems when adjacent elements are exactly co-planar. The difficulty is overcome by providing a fictitious torsional spring along the local normal direction at each node of element. However, this technique has the drawback that it interferes with the ability of the element to undergo strain free rigid body motions.

Kanok-Nukulchai (1979) used an additional constraint to link the torsional rotation (φ_t) to the average in-plane rotation of the mid-surface. Adopting the continuum mechanics definition, the constraint equation can be written as

$$E_d = \varphi_t - \frac{1}{2}\left(\frac{\partial v}{\partial r} - \frac{\partial u}{\partial s}\right) = 0 \tag{39}$$

In practice, because the above Eq. (39) will make the element stiffness too stiff, using the penalty function approach the amount of strain energy that corresponds with the drilling strain can be adjusted to the appropriate level. The first drilling stiffness matrix ($\boldsymbol{K}_{D1}$) associated with E_d is given by

$$\boldsymbol{K}_{D1} = \varpi_1 Gh\int_s \boldsymbol{B}_d^T \boldsymbol{B}_d dS \tag{40}$$

where G is the shear modulus, ϖ_1 is a penalty function constant and the strain-displacement matrix relation is as follows:

$$\boldsymbol{B}_d = \sum_{i=1}^{8}\left[\frac{1}{2}(g^i \boldsymbol{V}_r - f^i \boldsymbol{V}_s) \quad H^i \boldsymbol{V}_t\right] \tag{41}$$

In addition, a very soft rotational spring, aligned with local normal at each gauss point, may be used. This leads to the second stiffness matrix ($\boldsymbol{K}_{D2}$) for the drilling degree of freedoms.

$$\boldsymbol{K}_{D2} = \varpi_2 \int_s \boldsymbol{V}_t \boldsymbol{V}_t^T dS \tag{42}$$

where ϖ_2 is spring stiffness. Then, the two stiffness matrices of drilling degree of freedom can be added to the linear stiffness matrices. The adding of the two stiffness to restrain the torsional mode produces a convergence solution in the curved shell which the membrane effect is significant.

3. Numerical example

The general purpose package (FINAS) was developed in Imperial college, London for the nonlinear analysis of thin-walled structures on a UNIX environment. At present, the development of an extended version of **FINAS,** named as **XFINAS**, is on going at AIT. The new version will include non-linear dynamic analysis and will run on the Window 2000 Operating System in a personal computer.

The patch test, distortion test and other various numerical tests of the present shell element named as SHELL8* are carried out and validated using **XFINAS**. All the results of the shell element showed very good agreement with references. Several examples are given to demonstrate the efficiency and accuracy of the present shell element. Most of the results presented here are normalized with the analytical solution, i.e., the ratio of the values obtained from SHELL8* to the theoretical values. The analysis data are reduced to a letter grade by the following rule proposed by MacNeal and Harder (1985), as follows:

Grade	Rule
A	2 % $\geq$ error
B	10 % $\geq$ error $\geq$ 2%
C	20 % $\geq$ error $\geq$ 10 %
D	50 % $\geq$ error $\geq$ 20 %
F	error > 50 %

3.1 Morley hemispherical shell with 18° hole problem

MacNeal and Harder (1985) proposed the hemispherical shell problem for the validation of shell elements, which is shown in Fig. 5. The results are shown in Table 2. The value of the displacement at the loading point given by MacNeal and Harder (1985) is 0.094. As noted for this problem, the membrane locking is more severe than the shear locking. This problem is a challenging test to the ability of a shell element to overcome membrane locking over most of the shell. Because of the symmetry, only one quadrant of the problem is modeled. In contrast to poor performance of the NASTRAN QUAD8 using full integration, the solution using reduced integration has better performance, but shows convergence over the unit value. The comparison of the normalized displacement of the SHELL8* solution with the solution given by in the references shows that the
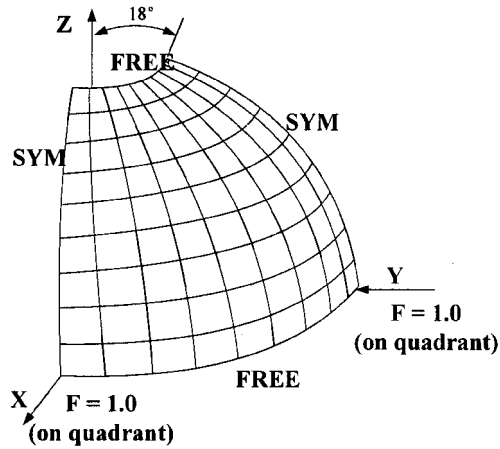

Fig. 5 Spherical shell, radius = 10.0 : thickness = 0.04, $E = 6.825 \times 10^7$, $\nu = 0.22$; mesh = $N \times N$, loading : concentrated forces

Table 2 Hemispherical shell with 18 degree hole problem

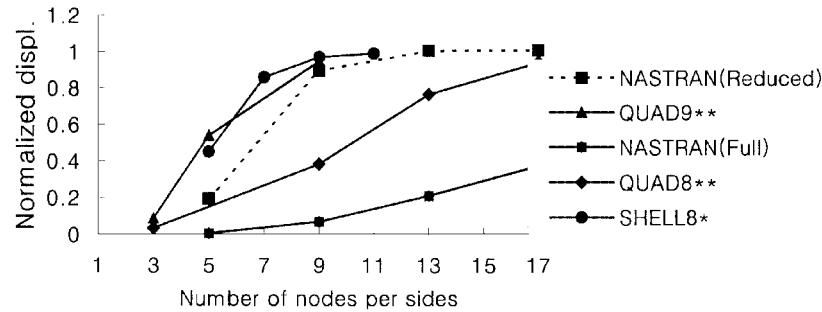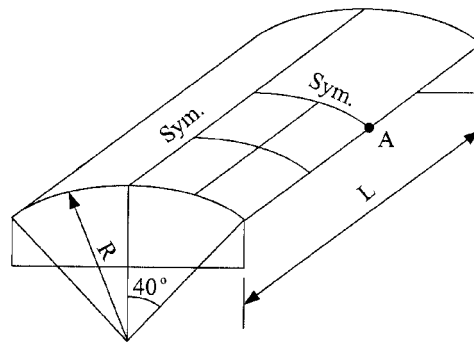| QUAD8:Full [MacNeal]	QUAD8:Reduced [MacNeal]	QUAD8** [Lakshminaryana & Kailashi]	QUAD9** [Huang & Hinton]	SHELL8* [XFINAS]
0.006 (4×4)	0.194 (4×4)	0.034 (2×2)	0.0863 (2×2)	0.45 (4×4)
0.069 (8×8)	0.895 (8×8)	0.383 (8×8)	0.538 (4×4)	0.86 (6×6)
0.210 (12×12)	1.005 (12×12)	0.765 (12×12)	0.948 (8×8)	0.97 (8×8)
0.373 (16×16)	1.008 (16×16)	0.940 (16×16)		0.99 (10×10)

Fig. 6 Mesh convergence of Morley hemispherical shell

Fig. 7 Scordelis-Lo roof = 25.0; length = 50.0; thickness = 0.25; $E = 43.2 \times 10^8$, $v = 0.0$; loading; 90.0/unit area

Table 3 Deflection at center of free edge of Scordelies-Lo's roof

QUAD8:Full [MacNeal]	QUAD8:Reduced [MacNeal]	QUAD 8** [Lakshminaryana & Kailashi]	MITC8 [Bathe & Dvorkin]	SHELL8* [XFINAS]
0.486 (4×4)	0.984 (4×4)	0.8739 (2×2)	1.15 (2×2)	0.747 (2×2)
0.841 (8×8)	0.997 (8×8)	0.9762 (4×4)	1.005 (4×4)	0.99 (4×4)
0.956 (12×12)	0.996 (10×10)	0.9787 (8×8)	1.0003 (8×8)	1.0 (8×8)

SHELL8* formulation performs better than the others.

3.2 Scordelis-Lo roof problem

The Scordelis-Lo roof under uniformly distributed load is shown in Fig. 7. This problem is useful in evaluating the ability of an element to deal with complex states of membrane strain. The exact solution is 0.3024 as quoted from MacNeal and Harder (1985). Because of symmetry, only one quarter of the problem is modeled. The normalized vertical deflection at point A is given in Table 3. Similar to the results of the hemispherical shell, the results of NASTRAN QUAD8 (in reference by MacNeal, 1994) using the reduced integration is better than that using full integration, but it shows
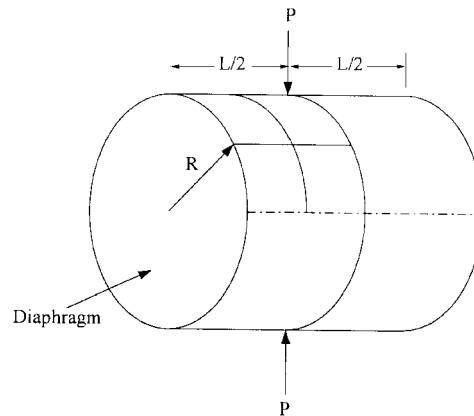
Fig. 8 Pinched cylinder with rigid end diaphragm ($R = 300.$, $L = 600.$, $E = 3.0 \times 10^6$, $v = 0.3$, $h = 3.0$, $P = 1.0$)

Table 4 Pinched cylinder with diaphragm

MITC8 [Bathe & Dvorkin]	9-node shell [Belytschko *et al.*]	S9R5 [ABAQUS]	SHELL8* [XFINAS]
0.952 (5×5)	0.737 (4×4)		0.657 (4×4)
0.990 (8×8)	0.961(8×4)		0.862(8×4)
0.999 (10×10)	0.999(16×4)	1.004 (9×9)	0.997 (8×8)

an oscillating convergence. The result in Table 3 shows very good performance of the proposed element in contrast to references.

3.3 Pinched cylinder with end diaphragms problem

The pinched cylinder with end diaphragms is shown in Fig. 8. This is one of the most severe tests of an element's ability to model both inextensional bending and complex membrane states. Belytschko *et al.* (1989) pointed out the difficulty in passing this test and quoted that an element that passes the diaphragm support test problem will perform well when the boundary condition is simplified to a free boundary. The exact solution is 0.18248×10^4. The displacement normalized to the exact solution in Table 4 showed that the present shell element does not suffer from both shear and membrane locking and converged faster.

3.4 Plate bending problem with clamped boundary condition

The clamped rectangular plates subjected to a uniform distributed loading are carried out for aspect ratio of 1.0. The plates are modeled by employing quarter symmetry. The finite element mesh of 4×4 elements is used for all the cases. In order to identify the limitation of shear locking due to the thickness, linear analysis with various cases of thickness is carried out. The central deflection

theory from thin plate theory with clamped edges by Timoshenko and Woinowosky-Krieger (1959) is

$$\delta = \frac{0.00126qa^4}{D} = 0.72576E - 3$$

where q is a uniform loading intensity, a is length and D is rigidity.

Table 5 shows the performance of the proposed element is good in the case of very thin plates with an aspect ratio 1.0. Since the thickness is reduced as very thin, the solutions using the full integration become deviated in comparison with the analytical solutions. However, the solution using the reduced integration based on the energy control formulation by Kim (1998) and showed very good performance in very thin plates. The above Table suggested guide lines for the case of

Table 5 The normalized plate bending solution with clamped edges

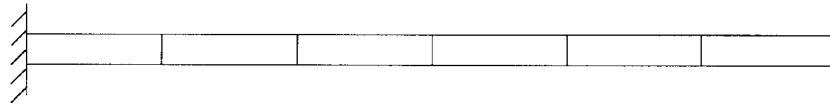| Thickness ratio	SHELL8* (Reduced)	SHELL8* (Full)
$h/a = 0.01$	1.002	0.992
$h/a = 0.009$	1.002	0.989
$h/a = 0.008$	1.002	0.985
$h/a = 0.007$	1.002	0.979
$h/a = 0.006$	1.002	0.970
$h/a = 0.005$	1.002	0.956
$h/a = 0.004$	1.002	0.930
$h/a = 0.003$	1.002	0.888
$h/a = 0.002$	1.002	0.770
$h/a = 0.001$	1.002	0.50

Fig. 9 Tip displacement of a cantilever beam: length = 6.0, width = 0.5; $h = 0.1$, $E = 1.0 \times 10^7$, $v = 0.3$
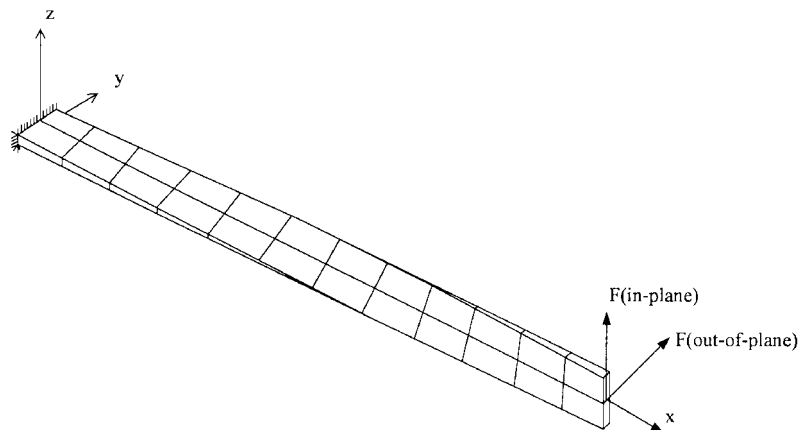

Fig. 10 Twist beam length = 12.0, width = 1.1; depth = 0.32; twist = 90°, $E = 29.0 \times 10^6$; $v = 0.22$; mesh = 12×2

plate bending problems. Again the proposed element for plate bending problems showed good performance for clamped edges.

3.5 Cantilever beam problem

MacNeal and Harder (1985) suggested three separate cantilever beam tests that evaluate sensitivity to various deformation patterns and distortions of the element geometry, i.e., a) a straight beam, b) a curved beam and c) a twisted beam. Descriptions of the straight and twisted beam problems are provided in Fig. 9 and Fig. 10. Benchmark solutions are also given in Table 6.

3.5.1 Straight beam problem

A cantilever beam with a 6×1 mesh is tested to investigate the proposed element by employing four different loadings, i.e., a) extension loading, b) in-plane loading, c) out-of-plane loading and d) twisting, at the free end.

Table 7 summarizes the solutions of tests in comparison with the references. This element performs well for extension and out of plane shear loading, and in-plane shear and twisting loading are close to exact solution.

3.5.2 Twisted beam problem

Table 6 Benchmark solutions for beam problems [MacNeal and Harder]

Tip load direction	Displacement in direction of load	
	Straight beam	Twisted beam ($t = 0.32$)
Extension	3.0×10^{-5}	-
In-plane shear	0.10810	0.005424
Out-of-plane shear	0.43210	0.001754
Twist	3.208×10^{-4}	-

Table 7 Result of straight Cantilever beam

Problems	QUAD8:Reduced [MacNeal]	QUAD8** [Lakshminaryana & Kailashi]	SHELL8* [XFINAS]
Extension	0.999	0.998	0.997
In-plane shear	0.987	0.985	0.964
Out of plane shear	0.991	0.996	0.980
Twist	0.95	0.944	0.940

Table 8 Result of twisted Cantilever beam

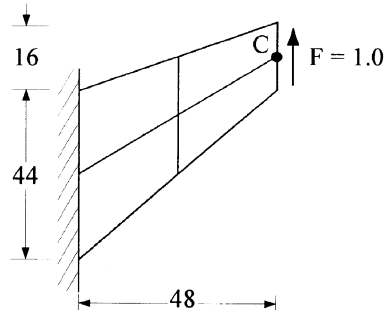| Problems	QUAD8 [MacNeal]	QUAD8** [Lakshminaryana & Kailashi]	SHELL8* [XFINAS]
In-plane shear	0.998	0.993	0.989
Out of plane shear	0.998	0.985	0.996

Fig. 11 Cook's tapered and swept panel problem, $E = 1.0$; $v = 1/3$; $h = 1.0$

Table 9 Result of Cook's beam

4-node shell by Simo *et al.*	9 node shell [Ma]	SHELL8* [XFINAS]
0.883 (4×4)	0.930 (2×2)	0.961 (4×4)
0.963 (16×16)	0.985 (4×4)	0.990 (6×6)
0.991 (64×64)	0.998 (8×8)	1.0 (8×8)

The twisted beam in Fig. 10 was subjected to two loading conditions, i.e., a) in-plane loading and b) out-of-plane loading, at free end to test the effect of element warping. Table 8 shows very good performance of the proposed element both loading cases.

3.6 Cook's tapered and swept panel problem

The tapered and swept panel with one edge clamped and the other edge loaded by a distributed shear force was analyzed to further test the in-plane behaviour of the proposed element.

This problem was used by Cook and many other researchers to test the sensitivities of finite elements due to geometric distortions. The reference solution for the vertical displacement at point *c* is taken to be 23.90 (Yunus *et al.* 1989). While results of all the elements considered converge to the reference solution, very good solutions of the proposed element are shown in Table 9.

3.7 A simply supported laminated spherical shells under a uniform pressure.

The linear analysis of double curved laminated composite shells under a uniform loading is carried out using 4×4 meshes. The shells have simply supported boundary conditions. The lay-up considered are nine layers cross-ply (0°/90°/0°/90°/0°/90°/0°/90°/0°) shells. One is with the total thickness $h = 0.01$ m and the other is with $h = 0.001$ m. The radius of the curved panel is $R = 10$ m. The geometric and material data of graphite/epoxy composite used are:

$$E_L = 2.67 \times 10^{11} \text{ N/mm}^2, \ E_T = 5.1713 \times 10^9 \text{ N/mm}^2$$
$$G_{LT} = 3.1028 \times 10^9 \text{ N/mm}^2, \ G_{13} = G_{23} = 2.5856 \times 10^9 \text{ N/mm}^2, \ v_{LT} = 0.25$$

Table 10 The non-dimensional center displacement of spherical shells for cross-ply laminate

h/a	4 node shell [Wang & To]	4 node shell [Somashekar et al.]	SHELL8* [XFINAS]	Analytical sol. [Noor & Mathers]
0.01 ($f_0 = 1.0 \times 10^3$)	2.717×10^{-5}	2.727×10^{-5}	2.723×10^{-5}	2.713×10^{-5}
0.001 ($f_0 = 1.0$)	5.89×10^{-5}	5.985×10^{-5}	5.864×10^{-5}	5.916×10^{-5}
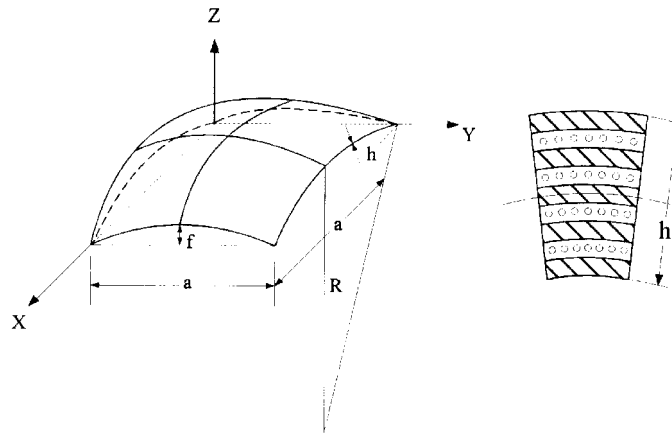
Fig. 12 The double curved spherical shell segment, $R = 10$ m, $a = 1.0$ m, $h = 001$ m, 0.001 m

The load intensity $f_0 = 1.0 \times 10^3$ N/m^2 for the thick panel and $f_0 = 1.0$ N/m^2 is for the thinner shell panel. One quarter of the laminated shell panel is modeled. And the center deflection of the shell panel using 4×4 meshes is compared with the non-dimensional form $(W = W_c E_L h^3 / f_0 a^4)$. The present results show very good agreement with analytical solutions in the thin shells.

4. Conclusions

In order to improve the previous work by Kim *et al.* (1998) and Kim & Vojiadjis (1999), a new eight-node assumed strain shell element is developed for linear analysis of beam, plate and shell structures. The present assumed strain method completely removed both membrane and shear locking behavior even when full integration is used in the formulation. In contrast to MITC8 of ADINA and QUAD8 of NASTRAN, this element is accurate and computationally efficient due to the explicit integration through the thickness. In addition, this explicit formulation can be extended for nonlinear analysis and significantly reduce the computational time. The introduction of an explicit transformation scheme in the constitutive equation makes it possible to deal with both isotropic and orthotropic materials. The present formulation is well compatible with the drilling degree of freedom, which can be used the modeling of the stiffened shell structures. From several numerical examples, the present shell element shows better performance in compared with other shell elements. The present assumed strain methods could be easily implemented into finite element code and used for the practical purpose. The future work will address the extension this work to the nonlinear static and dynamic analysis of shell structures and improved transverse shear deformation

study of composite laminate structures.

Acknowledgements

The author greatly acknowledge Mr. Hari for his computational work at the Asian Institute of Technology.

References

ABAQUS Example problem Manual (1994), **1**.

Ahmad, S., Irons, B.M. and Zienkiewicz, O.C. (1970), "Analysis of thick and thin shell structures by curved finite elements", *Int. J. Numer. Meth. Engng.*, **2**, 419-451.

Bathe, K.J. and Dvorkin, E.N. (1986), "A formulation of general shell elements-the use of mixed interpolation of tensorial components", *Int. J. Numer. Meth. Engng.*, **22**, 697-722.

Belytschko, T., Wong, B.L. and Stolarski, H. (1989), "Assumed strain stabilization procedure for the 9-node lagrangian shell element", *Int. J. Numer. Meth. Engng.*, **28**, 385-414.

Choi, C.K. and Yoo, S.W. (1991), "Geometrically nonlinear behaviour of an improved degenerate shell element", *Computers and Structures*, **40**(3), 785-794.

FINASIC User Manual, (1990), Department of Civil Engineering, Imperial College, London.

Haitao, Ma. (1990), "Development of a geometrically nonlinear shell element by assumed strain methods", Asian Institute of Technology, Dr. Thesis.

Huang, H.C. and Hinton, E. (1986), "A new nine node degenerated shell element with enhanced membrane and shear interpolation", *Int. J. Numer. Meth. Engng.*, **22**, 73-92.

Kebari, H. and Cassel, A.C. (1992), "A stabilized 9-node non-linear shell element", *Int. J. Numer. Meth. Engng.*, **35**, 37-61.

Kanok-Nukulchai, W. (1979), "A simple and efficient finite element for general shell analysis", *Int. J. Numer. Meth. Engng.*, **14**, 179-200.

Kim, K.D. (1992), "Non-linear analysis of fibre-reinforced composite structures using finite elements", Ph.D. Thesis, Dept. of Civil Engineering, Imperial College, London.

Kim, K.D., Park, T. and Voyiadjis, G.Z. (1998), Postbuckling, "Analysis of composite panels with imperfection damage", *Computational Mechanics*, **22**, 375-387.

Kim, K.D. and Voyiadjis, G.Z. (1999), "Non-linear finite element analysis of composite panels", *Composites Part B: Engineering*, **30**(4), 383-394.

Lakshminaryana, H.V. and Kailashi, K. (1989), "A shear deforamble curved shell element of quadrilateral shape", *Computers and Structures*, 987-1001.

Lee, S.J. and Kanok-Nukulchai, W. (1998), "A nine-node assumed strain finite element for large deformation analysis of laminated shells", *Int. J. Numer. Meth. Engng.*, **42**, 777-798.

Ma, H. and Kanok-Nukulchai, W. (1989), "On the application of assumed strained methods", in Kanok-Nukulchai *et al.* (eds.), Structural Engineering and Construction: Achievements, Trends and Challenges, 1168-1175.

MacNeal, R.H. and Harder, R.L. (1985), "A proposed standard set of problems to test finite element accuracy", *Finite Elements Analysis and Design*, **11**, 3-20.

MacNeal, R.H. (1994), *Finite Elements: Their Design and Performance*, Marcel Dekker., INC.

Noor, A.K. and Mathers, M.D. (1976), "Anisotropy and shear deformation in laminated composite plates", *AIAA*, **14**, 282-285.

Reddy, J.N. (1987), "A generalization of two-dimensional theories of laminated composite plates", *Commun. Appl. Numer. Methods*, **3**, 173-180.

Rolfes, R. and Rohwer, K. (1997), "Improved transverse shear stress in composite finite element based on first

order shear deformation theory", *Int. J. Numer. Meth. Engng.*, **40**, 51-60.

Simo, J.C., Fox, D.D. and Rifai, M.S. (1989), "A stress resultant geometrically exact shell model, part II the linear theory; computational aspects", *Computer Methods in Applied Mechanics and Engineering.*, **73**, 53-92.

Somashekar, B.R., Prathap, G. and Ramesh Babu, C. (1987), "A field-consistent, four-noded, laminated, anisotropic plate/shell element", *Computers and Structures*, **25**(3), 345-353.

Timosenko, S.P. and Woinowosky-Krieger, S. (1959), *Theory of Plates and Shells*, McGraw-Hill Kogakusa.

To, C.W.S. and Wang, B. (1998), "Hybrid strain-based three-node flat triangular laminated composite shell elements", *Finite Elements Analysis and Design*, **28**, 177-207.

Yunus, S.M., Saigal, S. and Cook, R.D. (1989), "On improved hybrid finite elements with rotational degree of freedom", *Int. J. Numer. Meth. Engng.*, **28**, 785-800.

Appendix 1

The local coordinate is expressed as $r = \sum_{i=1}^{8} H^i(\xi, \eta) r^i$ and $s = \sum_{i=1}^{8} H^i(\xi, \eta) s^i$.

$$\frac{\partial r}{\partial \varsigma} = \frac{\partial s}{\partial \varsigma} = 0 \qquad \frac{\partial t}{\partial \varsigma} = \frac{h}{2} \tag{43}$$

From Eq. (22), the transverse shear strain $e_{\xi\varsigma}$ can be expanded as follows:

$$
\begin{aligned}
e_{\xi\varsigma} &= \frac{\partial x^i}{\partial \xi}\frac{\partial x^j}{\partial \varsigma} e_{ij} \\
&= \frac{\partial r}{\partial \xi}\frac{\partial x^j}{\partial \varsigma} e_{rj} + \frac{\partial s}{\partial \xi}\frac{\partial x^j}{\partial \varsigma} e_{sj} + \frac{\partial t}{\partial \xi}\frac{\partial x^j}{\partial \varsigma} e_{tj} = \frac{\partial r}{\partial \xi}\frac{\partial t}{\partial \xi} e_{rt} + \frac{\partial s}{\partial \xi}\frac{\partial t}{\partial \xi} e_{st} + \frac{\partial t}{\partial \xi}\frac{\partial t}{\partial \xi}e_{tt}\ ^{0} \\
&= \frac{\partial r}{\partial \xi}\frac{h}{2} e_{rt} + \frac{\partial s}{\partial \xi}\frac{h}{2} e_{st}
\end{aligned}
$$

$$e_{\eta\varsigma} = \frac{\partial r}{\partial \eta}\frac{h}{2} e_{rt} + \frac{\partial s}{\partial \eta}\frac{h}{2} e_{st} \tag{44}$$

Appendix 2

$$
\begin{aligned}
e_{\xi\xi} &= \frac{\partial x^i}{\partial \xi}\frac{\partial x^j}{\partial \xi} e_{ij} \\
&= \frac{\partial r}{\partial \xi}\frac{\partial r}{\partial \xi} e_{rr} + \frac{\partial r}{\partial \xi}\frac{\partial s}{\partial \xi} e_{rs} + \frac{\partial r}{\partial \xi}\frac{\partial t}{\partial \xi}e_{rt}\ ^{0} + \frac{\partial s}{\partial \xi}\frac{\partial r}{\partial \xi} e_{sr} + \frac{\partial s}{\partial \xi}\frac{\partial s}{\partial \xi} e_{ss} + \frac{\partial s}{\partial \xi}\frac{\partial t}{\partial \xi}e_{st}\ ^{0} \\
&\quad + \frac{\partial t}{\partial \xi}\frac{\partial r}{\partial \xi}e_{tr}\ ^{0} + \frac{\partial t}{\partial \xi}\frac{\partial s}{\partial \xi}e_{ts}\ ^{0} + \frac{\partial t}{\partial \xi}\frac{\partial t}{\partial \xi}e_{tt}\ ^{0} \\
&= \frac{\partial r}{\partial \xi}\frac{\partial r}{\partial \xi} e_{rr} + \frac{\partial s}{\partial \xi}\frac{\partial s}{\partial \xi} e_{ss} + 2\frac{\partial r}{\partial \xi}\frac{\partial s}{\partial \xi} e_{rs}
\end{aligned} \tag{45}
$$

With a similar method

$$e_{\eta\eta} = \frac{\partial r}{\partial \eta}\frac{\partial r}{\partial \eta} e_{rr} + \frac{\partial s}{\partial \eta}\frac{\partial s}{\partial \eta} e_{ss} + 2\frac{\partial s}{\partial \eta}\frac{\partial r}{\partial \eta} e_{rs}$$

$$e_{\xi\eta} = \frac{\partial r}{\partial \xi}\frac{\partial r}{\partial \eta} e_{rr} + \frac{\partial s}{\partial \xi}\frac{\partial s}{\partial \eta} e_{ss} + \left(\frac{\partial r}{\partial \xi}\frac{\partial s}{\partial \eta} + \frac{\partial s}{\partial \xi}\frac{\partial r}{\partial \eta}\right) e_{rs} \tag{46}$$

Appendix 3

$$\left\{ \begin{matrix} \sigma_1 \\ \sigma_2 \\ \sigma_{12} \end{matrix} \right\}^k = \begin{bmatrix} C_{11} & C_{12} & 0 \\ C_{11} & C_{22} & 0 \\ 0 & 0 & C_{33} \end{bmatrix}^k \left\{ \begin{matrix} \hat{e}_1 \\ \hat{e}_2 \\ \hat{e}_{12} \end{matrix} \right\}^k \tag{47}$$

$$\left\{ \begin{matrix} \sigma_{13} \\ \sigma_{23} \end{matrix} \right\}^k = \begin{bmatrix} C_{44} & 0 \\ 0 & C_{55} \end{bmatrix}^k \left\{ \begin{matrix} \hat{e}_{13} \\ \hat{e}_{23} \end{matrix} \right\}^k \tag{48}$$

where the stiffness coefficients of C_{ij} are defined as follows:

$$C_{11} = \frac{E_L}{(1 - \nu_{LT}\nu_{TL})}$$

$$C_{12} = \frac{E_L\nu_{TL}}{(1 - \nu_{LT}\nu_{TL})}$$

$$C_{22} = \frac{E_T}{(1 - \nu_{LT}\nu_{TL})}$$

$$C_{33} = G_{TL}$$

$$C_{44} = G_{13}$$

$$C_{55} = G_{23} \tag{49}$$

Since, composite structures are typically built up with the fibre directions of each layer orientated at different angles, the following transformed stress and strain relations apply for a lamina orientated at an angle ϑ with respect to a general coordinate system *r-s*.

$$\left\{ \begin{matrix} \sigma_r \\ \sigma_s \\ \sigma_{rs} \end{matrix} \right\}^k = \begin{bmatrix} \overline{C}_{11} & \overline{C}_{12} & \overline{C}_{13} \\ \overline{C}_{21} & \overline{C}_{22} & \overline{C}_{23} \\ \overline{C}_{31} & \overline{C}_{32} & \overline{C}_{33} \end{bmatrix}^k \left\{ \begin{matrix} \hat{e}_r \\ \hat{e}_s \\ \hat{e}_{rs} \end{matrix} \right\}^k$$

where $$\left\{ \begin{matrix} \sigma_{rt} \\ \sigma_{st} \end{matrix} \right\}^k = \begin{bmatrix} \overline{C}_{44} & \overline{C}_{45} \\ \overline{C}_{54} & \overline{C}_{55} \end{bmatrix}^k \left\{ \begin{matrix} \hat{e}_r \\ \hat{e}_{st} \end{matrix} \right\}^k \tag{50}$$

$$\overline{C}_{11} = C_{11}m^4 + 2(C_{12} + 2C_{33}m^4)m^2n^2 + C_{22}n^4$$

$$\overline{C}_{12} = \overline{C}_{21} = (C_{11} + C_{22} + 4C_{33})m^2n^2 + C_{12}(m^4 + n^4)$$

$$\overline{C}_{13} = \overline{C}_{31} = -mn^3C_{22} + m^3nC_{11} - mn(m^2 - n^2)(C_{12} + 2C_{33})$$

$$\overline{C}_{22} = C_{11}n^4 + 2(C_{12} + 2C_{33}m^4)m^2n^2 + C_{22}m^4$$

$$\overline{C}_{44} = C_{44}m^2 + C_{55}n^2$$

$$\overline{C}_{55} = C_{44}n^2 + C_{55}m^2$$

$$\overline{C}_{45} = \overline{C}_{54} = (C_{55} - C_{44})mn \tag{51}$$

and *m* and *n* in Eq. (51) are

$$m = \cos\vartheta$$
$$n = \sin\vartheta \tag{52}$$

where ϑ is a fibre angle.

Notation

$^{-}$	: bar over : value measured at midsurface
x, y, z	: global coordinate system
r, s, t	: local coordinate system
ξ, η, ς	: natural coordinate system
i	: superscript referring to node number i
m, b, q	: subscript referring to membrane, bending and transverse shear respectively
$\boldsymbol{P}$	: position vector
H^i	: shape function at node i
$\boldsymbol{T}$	: direction cosine of the new local axes with respect to the global axes
$\overline{\boldsymbol{U}} = (\overline{U}, \overline{V}, \overline{W})$	: global translation of the midsurface
$\boldsymbol{\theta} = (\theta_x, \theta_y, \theta_z)$	: global rotation of the midsurface
$\overline{\boldsymbol{u}} = (\overline{u}, \overline{v}, \overline{w})$	: local translation of the midsurface
$\varphi = (\varphi_r, \varphi_s, \varphi_t)$	: local rotation of the midsurface
$\boldsymbol{U} = (\overline{\boldsymbol{U}}, \theta)$	: global displacement
$u = (\overline{\boldsymbol{u}}, \varphi)$	: local displacement
$\boldsymbol{V}_r, \boldsymbol{V}_s, \boldsymbol{V}_t$	: base vector tangential to the local co-ordinates
$\boldsymbol{e}_m, \boldsymbol{e}_b, \boldsymbol{e}_q$	: linear part of the membrane, bending and transverse shear strain vector
$\gamma_{\xi\varsigma}, \gamma_{\eta\varsigma}$	: transverse shear strains in the natural coordinates
$\boldsymbol{N}, \boldsymbol{M}, \boldsymbol{Q}$	: resultant membrane forces (N_r, N_s, N_{rs}), moments (M_r, M_s, M_{rs}), and transverse shear forces (Q_r, Q_s)
$\boldsymbol{A}, \boldsymbol{B}, \boldsymbol{D}, \overline{\boldsymbol{A}}$	: membrane, membrane-bending, bending and transverse stiffness matrix respectively
C_{ij}	: material stiffness tensor
$\boldsymbol{K}_e$	: element stiffness matrix
dS	: surface area element
E_L, E_T	: Young's modulus along longitudinal (L) and transverse (T) axes of a single lamina.
G_{LT}	: in-plane shear modulus of a single lamina
G_{13}, G_{23}	: transverse shear modulus in the plane 1-3 and 2-3
ν, ν_{LT}	: Poisson's ratio